MAGNETIC PROPERTIES OF A MIXED SPIN-1/2 AND SPIN-7/2 HEXAGONAL CORE-SHELL NANOTUBE

H. SAADI[1,*], E. M. JALAL[1,2], O. ELGARRAOUI[1], A. EL ANTARI[1], M. MADANI[3], M. EL BOUZIANI[1]

[1]Theoretical Physics Group, Laboratory L.P.M.C., Faculty of Sciences, Chouaib Doukkali University, El Jadida, Morocco

[2]LS2ME Laboratory, Polydisciplinary faculty of Khouribga, Sultan Moulay Slimane University, Beni Mellal, Morocco

[3]Department Physics-Chemistry, CRMEF, Meknes, Morocco

Compiled May 4, 2023

The magnetic properties and phase diagrams of a hexagonal nanotube with core-shell structure have been examined within the framework of the mean field theory based on the Bogoliubov inequality as well as the Monte Carlo simulation via the Metropolis algorithm. We have studied in detail the influences of the different exchange couplings and the crystal field on the phase diagrams of the system. This study allowed us to discover the existence of interesting critical phenomena, in particular the compensation behavior. Moreover, we have investigated the behavior of the magnetizations corresponding to each of the phase diagrams in order to verify the obtained results.

Key words: Hexagonal nanotube, Core-shell structure, Mixed spins, Compensation, Phase diagram..

PACS: 05.10.Ln, 64.60.De, 75.10.Dg, 75.10.Hk, 75.40.Cx, 75.40.Mg, 75.50.Gg, 75.60.Ej, 75.75.+a

1. INTRODUCTION

Nanostructures characterized by their small size, such as nanotubes, nanoparticles and nanowires, are presently the subject of the active researches, not only because of their fascinating physical properties [1] but also because of their potential application in different technological fields, for instance, permanent magnets, sensors, medical applications, ultra-high-density magnetic storage devices and environmental remediation [2–8]. In particular, magnetic nanotubes attracted more attention after the initial discovery of carbon nanotubes by the Japanese physicist Sumio Ijima [9], either experimentally or theoretically.

Experimentally, many magnetic nanotubes such as, CoNi nanotubes [10], FeNi nanotubes [11], Ni nanotubes [12], CoPt nanotubes [13], Bi2Te3 nanotubes [14], and FeCo nanotubes [15]..., have been successfully elaborated using a variety of manu-

*Corresponding author: saadi.h@ucd.ac.ma

facturing methods, among which we cite, the wetting template method [11, 16] and the electrodeposition [10]. On the other hand, given that the theoretical study complements the experimental study in obtaining credible results and deep evidences, we find that some theoretical methods either analytical or simulation have studied this type of nanostructures, namely, effective field theory (EFT) [17–21], Monte Carlo simulation (MCS) [22–25], and mean field theory (MFT) [26]. Z. Elmaddahi et al [20], performed the effective field theory with correlations to examine certain characteristic behaviors of a hexagonal spin-3/2 Ising nanotube, namely, the magnetization, internal energy, susceptibility, and specific heat. It was shown that the system can exhibits a triple, two or single hysteresis loops. Also, employing the Monte Carlo simulation with the Metropolis algorithm, R. G. B. Mendes et al, analyzed the magnetic properties of a mixed spin-1/2 Ising model and spin-1 Blume-Capel model in a hexagonal nanotube two layers system [22]. They have observed the appearance of the first- and second-order phase transition lines. In addition, the magnetic properties of a decorated Ising nanotube have been studied by R. Masrour et al. using Monte Carlo Simulation [25].

Furthermore, we cannot talk about nanostructured systems without referring to the structures adopted to study them. One of the best structure is the core-shell, witch constituting of a central (core) surrounded by a shell surface. In remarkable, much effort has been dedicated to exploring the different magnetic properties of these systems. For example, by using the mean field approximation and Monte Carlo simulation, E.M Jalal et al. [27] have investigated the magnetic behaviors of the mixed spin-1/2 and spin-3/2 hexagonal Ising nanowire with core-shell under the impact of crystal field. Also, R. Masrour et al. [28], used the Monte Carlo simulations to study the effect of the crystal field and exchange interactions on the thermal magnetizations, the magnetic susceptibilities and magnetic hysteresis loops of a mixed spins (2, 1) hexagonal Ising nanowire with core-shell structure. Moreover, within the framework of Monte Carlo simulation, L.B.Drissi et al. [29] have explored the effects of parameters of the Hamiltonian on magnetic properties and hysteresis behaviors of a graphyne core/shell nanoparticles. Also, the magnetic properties of a mixed spin (3/2, 1/2) ferrimagnetic nanoparticle, with a cubic shape and core-shell structure have been studied by O. Dakir et al. [30], using the Monte Carlo simulation. Recently, in two different works N. Hachem et al. [31, 32], used the mean field approximation, to investigate the influences of the exchange interactions and crystal field on the magnetic properties of a ferrimagnetic mixed-spin (3/2, 1/2) hexagonal Ising nanotube with core-shell structure. We should mention that these works show very important phenomena, such as the compensation temperatures and the hysteresis loops with multiple shapes.

According to the best of our knowledge, there have been no studies on mixed spin (7/2, 1/2) hexagonal Ising nanotube with core-shell structure. For this reason

we aim to study the phase diagrams and magnetic properties of this system under the effect of exchange interactions and the crystal field, using two methods: mean field theory and Monte Carlo simulation. This paper is structured as follows: the model and methods employed are described in Section 2, the results and discussions are presented in Section 3, and finally, the Section 4 is devoted to the conclusion.

2. MODEL AND METHODS

We consider a ferrimagnetic hexagonal nanotube with a core-shell structure of mixed spin 1/2 and spin 7/2, as depicted in Fig. 1. The spins σ, which can take two values $\pm 1/2$, occupy the sites of the core, while the spins S, which can take eights values $\pm 1/2$, $\pm 3/2$, $\pm 5/2$ and $\pm 7/2$ occupy the sites of the shell surface. The latter is formed by N hexagonal layers. In each layer, there are eighteen spins divided as follows: six spins on the core and twelve on the surface shell (Fig. 1.b). Thus the number total of the spins in the system is $N_T = 18N$. Our system is described by the following Hamiltonian which can be written as:

$$H = -J_C \sum_{ij} \sigma_i \sigma_j - J_S \sum_{kl} S_k S_l - J_{in} \sum_{ik} \sigma_i S_k - D_S \sum_{k=1}^{12N} S_k^2 \qquad (1)$$

where J_C (> 0) and J_S (> 0) are the exchange interaction parameters between the two nearest-neighbor spins at the core and at the surface shell, respectively. J_{in} (< 0) designates the ferrimagnetic exchange interaction between the spins of the core and those of the surface shell. D_S is the crystal-field interaction constant of the spins $S = 7/2$ of the shell sublattice. Moreover, we have selected J_C as the reduced unit of energy and temperature ($k_B T$), so $J_C = 1$.

2.1. MEAN FIELD APPROXIMATION

To examine our model approximately using the Mean Field theory, we use the variational principle based on Bogoliobuv's inequality corresponds to free energy [33]:

$$F(H) = F_0(H_0) + \langle H - H_0 \rangle_0 = \phi \qquad (2)$$

where $F(H)$ is the true free energy of the system described by the Hamiltonian given in eq. (1). $F_0(H_0)$ is the average free energy of an effective Hamiltonian H_0 which relies on variational parameters, and $< H - H_0 >_0$ is the average value of the value $H - H_0$ over the ensemble presented by H_0.

We devide our nanotube into three sublattices (L_σ), (L_{S1}) and (L_{S2}), such that the sublattice (L_σ) is occupied by the spins $\sigma = 1/2$ in the core, while the two sublattices (L_{S1}) and (L_{S2}) are occupied by the spins $S = 7/2$ located, respectively

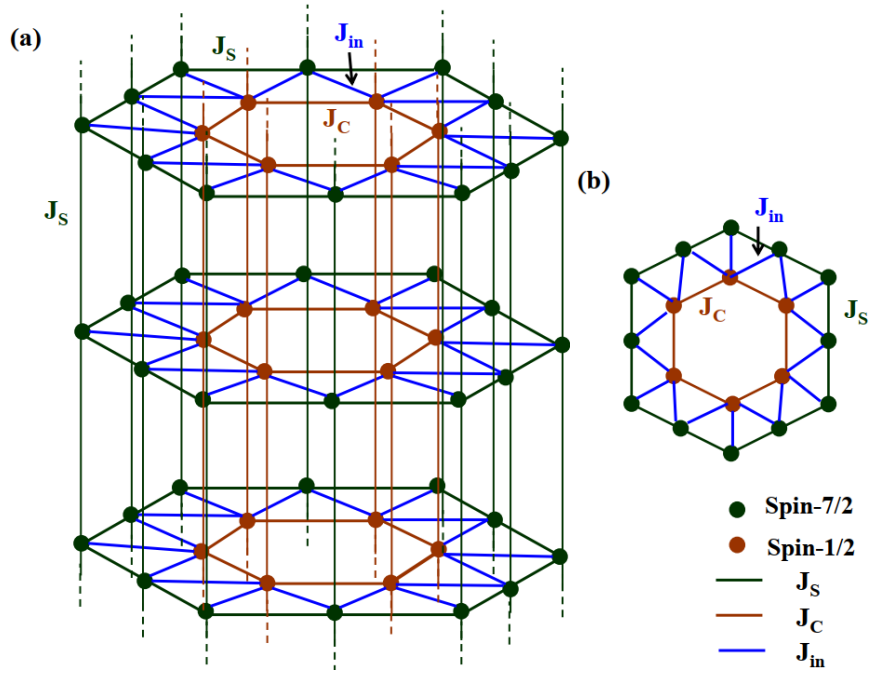

Fig. 1 – Schematic representation of a hexagonal nanotube with core-shell structure of mixed spin (7/2, 1/2) composed of the surface shell (green circles) and the core (brown circles) : (a) three-dimensional and (b) cross-section.

in the corners and in the middle of sides of the shell surface. So, we choose the effective Hamiltonian H_0 as follows:

$$H_0 = -\lambda_\sigma \sum_{i=1}^{6N} \sigma_i - \lambda_{S1} \sum_{k=1}^{6N} S_k - D_S \sum_{k=1}^{6N} S_k^2 - \lambda_{S2} \sum_{l=1}^{6N} S_l - D_S \sum_{l=1}^{6N} S_l^2 \qquad (3)$$

where λ_σ, λ_{S1} and λ_{S2} are the three variational parameters related the two different spins σ and S occupied the sublattices (L_σ), (L_{S1}) and (L_{S2}).

By calculating the free energy F_0 from the determination of the partition function Z_0 which are defined respectively by: and with $\beta = \frac{1}{k_B T}$ (k_B is the Boltzmann constant and T is the absolute temperature), we find the expression of the variational

free energy per site:

$$\begin{aligned}\phi =& -\frac{6N}{\beta}\ln\left\{2e^{\frac{49}{4}\beta D_S}\cosh\left(\frac{7}{2}\beta\lambda_{S1}\right)+2e^{\frac{25}{4}\beta D_S}\cosh\left(\frac{5}{2}\beta\lambda_{S1}\right)\right.\\ &\left.+2e^{\frac{9}{4}\beta D_S}\cosh\left(\frac{3}{2}\beta\lambda_{S1}\right)+2e^{\frac{1}{4}\beta D_S}\cosh\left(\frac{1}{2}\beta\lambda_{S1}\right)\right\}\\ &-\frac{6N}{\beta}\ln\left\{2e^{\frac{49}{4}\beta D_S}\cosh\left(\frac{7}{2}\beta\lambda_{S2}\right)+2e^{\frac{25}{4}\beta D_S}\cosh\left(\frac{5}{2}\beta\lambda_{S2}\right)\right.\\ &\left.+2e^{\frac{9}{4}\beta D_S}\cosh\left(\frac{3}{2}\beta\lambda_{S2}\right)+2e^{\frac{1}{4}\beta D_S}\cosh\left(\frac{1}{2}\beta\lambda_{S2}\right)\right\}\\ &-\frac{6N}{\beta}\ln\left\{2\cosh\left(\frac{1}{2}\beta\lambda_{\sigma}\right)\right\}+\lambda_{\sigma}m_C+\lambda_{S1}m_{S1}+\lambda_{S2}m_{S2}\\ &-2J_Cm_C^2-J_Sm_{S_1}^2-J_Sm_{S_2}^2-2J_Sm_{S_1}m_{S_2}-J_{in}m_Cm_{S_1}\\ &-2J_{in}m_Cm_{S_2}\end{aligned} \tag{4}$$

where m_C, m_{S_1} and m_{S_2} are the magnetizations per site of the sublattices (L_σ), (L_{S1}) and (L_{S2}) defined respectively by $m_C=\langle\sigma_i\rangle$, $m_{S_1}=\langle S_k\rangle$ and $m_{S_2}=\langle S_l\rangle$.

The minimization of the free energy per site with respect to the order and variational parameters allows us to obtain the following equations:

$$\begin{cases} m_C=\frac{1}{2}\tanh(\frac{1}{2}\beta\lambda_\sigma)\\ m_{S_1}=\frac{1}{2}\frac{7e^{\frac{49}{4}\beta D_S}\sinh(\frac{7}{2}\beta\lambda_{S_1})+5e^{\frac{25}{4}\beta D_S}\sinh(\frac{5}{2}\beta\lambda_{S_1})+3e^{\frac{9}{4}\beta D_S}\sinh(\frac{3}{2}\beta\lambda_{S_1})+e^{\frac{1}{4}\beta D_S}\sinh(\frac{1}{2}\beta\lambda_{S_1})}{e^{\frac{49}{4}\beta D_S}\cosh(\frac{7}{2}\beta\lambda_{S_1})+e^{\frac{25}{4}\beta D_S}\cosh(\frac{5}{2}\beta\lambda_{S_1})+e^{\frac{9}{4}\beta D_S}\cosh(\frac{3}{2}\beta\lambda_{S_1})+e^{\frac{1}{4}\beta D_S}\cosh(\frac{1}{2}\beta\lambda_{S_1})}\\ m_{S_2}=\frac{1}{2}\frac{7e^{\frac{49}{4}\beta D_S}\sinh(\frac{7}{2}\beta\lambda_{S_2})+5e^{\frac{25}{4}\beta D_S}\sinh(\frac{5}{2}\beta\lambda_{S_2})+3e^{\frac{9}{4}\beta D_S}\sinh(\frac{3}{2}\beta\lambda_{S_2})+e^{\frac{1}{4}\beta D_S}\sinh(\frac{1}{2}\beta\lambda_{S_2})}{e^{\frac{49}{4}\beta D_S}\cosh(\frac{7}{2}\beta\lambda_{S_2})+e^{\frac{25}{4}\beta D_S}\cosh(\frac{5}{2}\beta\lambda_{S_2})+e^{\frac{9}{4}\beta D_S}\cosh(\frac{3}{2}\beta\lambda_{S_2})+e^{\frac{1}{4}\beta D_S}\cosh(\frac{1}{2}\beta\lambda_{S_2})} \end{cases} \tag{5}$$

with:

$$\begin{cases} \lambda_\sigma=4J_Cm_C+J_{in}m_{S_1}+2J_{in}m_{S_2}\\ \lambda_{S_1}=J_{in}m_C+2J_Sm_{S_1}+2J_Sm_{S_2}\\ \lambda_{S_2}=2J_{in}m_C+2J_Sm_{S_1}+2J_Sm_{S_2} \end{cases}$$

Further, the magnetization per site corresponds to the surface shell and the total m_S magnetization per site M_T is written as:

$$\begin{cases} m_S=\frac{m_{S_1}+m_{S_2}}{2}\\ M_T=\frac{6m_C+12m_S}{18} \end{cases} \tag{6}$$

The compensation temperature T_{comp} of the system, exist if the sublattice magnetizations annul each other, which makes the total magnetization of the system decrease to zero. So the determination of this last can be gained by looking for the

intersection point between the some values of two sublattice magnetizations by employing:

$$|m_S(T_{comp})| = |m_C(T_{comp})| \tag{7}$$

$$sign(m_S(T_{comp})) = -sign(m_C(T_{comp})) \tag{8}$$

2.2. MONTE CARLO SIMULATION

To confirm the results getting by the mean field approximation, we utilize the Monte Carlo simulation based on the algorithm of Metropolis [34]. Thus, to simulate our nanotube defined by the Hamiltonian in Eq. (1), we randomly choose a configuration of spins and run tests to return to a single spin. In the x and y directions we apply the free boundary conditions while the periodic conditions are applied along the z axis. We carry out at each temperature, 10^5 Monte Carlo steps per site for calculating the averages of thermodynamic quantities, after discarding the first 3×10^4 steps per site to equilibrate the system.

The program calculates the magnetizations per site (m_C) and (m_S) of the core and shell, respectively, and the total magnetization per site M_T:

$$m_C = \frac{1}{N_C}\sum_{i=1}^{N_C}\sigma_i \qquad\qquad m_S = \frac{1}{N_S}\sum_{k=1}^{N_S}S_k \tag{9}$$

The total magnetization per site is calculated by the same formula (6) used in the MFT method. The compensation temperature is defined as the temperature at which:

$$N_C|m_S(T_{comp})| = N_S|m_C(T_{comp})| \tag{10}$$

where $N_C = 6N$ and $N_S = 12N$.

3. RESULTS AND DISCUSSION

We will dedicate this section to investigate the influence of the exchange interactions J_S, J_{in} and of the field D_S on the magnetic properties and phase diagrams of the studied system, using the two formulations described previously in section 2.

3.1. EFFECT OF THE SHELL EXCHANGE INTERACTION J_S

We begin our investigation by studying the impact of ferromagnetic shell coupling J_S/J_C on phase diagrams. In Fig. 2, the behavior of these phase diagrams is presented in the (J_S/J_C, T/J_C) plane using MFT and MCS, and for fixed values of $J_{in}/J_C = -0.2$ and $D_S/J_C = -2$.

As we observe, by increasing the value of J_S/J_C, the phase diagrams show a variation of phenomena. In fact, for all values of J_S/J_C, we can see that the phase

diagram obtained either by MFT or by MCS, displays that the ferrimagnetic and the paramagnetic phases are separated from each other by a second-order transition line. In addition, it is clear the appearance of the compensation temperature Tcomp, which occurs only for the small values of J_S/J_C, ($J_S/J_C \leq 0.75$ for MFT) and ($J_S/J_C \leq 0.5$ for MCS). Also, at low temperature and exactly in the ferrimagnetic region, we have three lines of first order transitions. The first one, which dissociates the ferrimagnetic phase $F_{11} \equiv (m_C = -1/2, m_S = 1/2)$ from the ferrimagnetic phase $F_{13} \equiv (m_C = -1/2, m_S = 3/2)$, the second one, dissociates the two ferrimagnetic phases $F_{13} \equiv (m_C = -1/2, m_S = 3/2)$ and $F_{15} \equiv (m_C = -1/2, m_S = 5/2)$, while the third one separates the two ferrimagnetic phases $F_{15} \equiv (m_C = -1/2, m_S = 5/2)$ and the $F_{17} \equiv (m_C = -1/2, m_S = 7/2)$ phase. Each of these three lines of first-order transition terminates at a critical end point E_1, E_2 and E_3 respectively. The coordinates of these critical end points are $E_1(J_S/J_C = 0.99,\ T/J_C = 2.11)$, $E_2(T/J_C = 0.988,\ T/J_C = 1.69)$ and $E_3(J_S/J_C = 0.995,\ T/J_C = 1.14)$ for MFT, while $E_1(J_S/J_C = 0.96,\ T/J_C = 0.468)$, $E_2(J_S/J_C = 0.959,\ T/J_C = 0.284)$ and $E_3(J_S/J_C = 0.96,\ T/J_C = 0.195)$ for MCS.

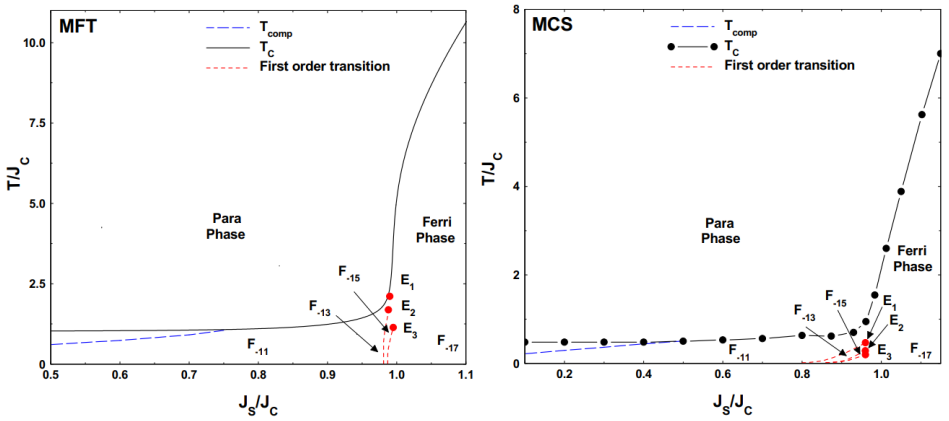

Fig. 2 – Phase diagrams of a nanotube system in the ($J_S/J_C, T/J_C$) plane when $J_{in}/J_C = -0.2$ and $D_S/J_C = -2$ by MFT and MCS.

In order to justify the construction of the phase diagrams plotted in Fig. 2. We present in the following some examples of the core magnetization m_C, the shell magnetization m_S and the total magnetization M_T of the nanotube as a function of the temperature, that explain us the phenomenon of compensation as well as first order transitions. From Fig. 3, and for $J_{in}/J_C = -0.2$, $D_S/J_C = -2$ and $J_S/J_C = 0.3$, we can observe for both methods, that the total magnetization curve displays two successive zero, the first one correspond to the compensation temperature T_{Comp}, and the second one correspond to the critical temperature T_C. While the two sublattices

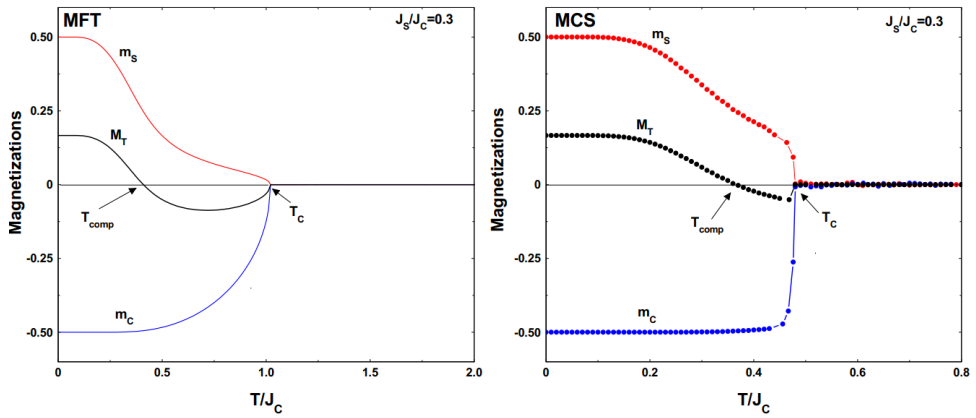

Fig. 3 – Sublattices magnetizations and the total magnetization and as a function of T/J_C for the case where $J_{in}/J_C = -0.2$, $D_S/J_C = -2$ and $J_S/J_C = 0.3$ by MFT and MCS.

magnetizations, after they have been reduced from their saturation value ($m_S = 0.5$ and $m_C = -0.5$), cancel each other out in a single zero corresponding to T_C. On the other hand, we notice that the values of T_C and T_{comp} obtained by the mean field method are greater than those obtained by the Monte Carlo simulation and this comes back to the fact that the mean field method ignores correlations between spins even if they are important near critical temperatures. Further, in the Fig 4, it is appears that the magnetizations curves m_S and M_T corresponding to the exchange interaction $J_S/J_C = 0.988$ for MFT and $J_S/J_C = 0.93$ for MCS, manifest three discontinuous jumps, indicating first-order transitions, firstly from ($m_S = 3.5$ and $m_C = -0.5$) to ($m_S = 2.5$ and $m_C = -0.5$), then from ($m_S = 2.5$ and $m_C = -0.5$) to ($m_S = 1.5$ and $m_C = -0.5$), and finally from ($m_S = 1.5$ and $m_C = -0.5$) to ($m_S = 0.5$ and $m_C = -0.5$).

It is remarkable to high-light that our results obtained under the effect of the ferromagnetic shell exchange interaction J_S/J_C can be qualitatively compared with other results found in other works, like; cylindrical or hexagonal nanotube with core-shell structure [31, 35, 36], nanoparticles with core-shell structure [30, 37], nanowire with core-shell structure [38, 40] and nanocube with core-shell structure [41]. Regarding each of the critical and compensation behaviors, we have found the same thing, but regarding the first-order transitions, the majority of these works do not find them, except for one that corresponds to the study of phase diagrams of mixed-spin (3/2, 1/2) hexagonal Ising nanotube with core-shell structure [31].

3.2. EFFECT OF THE CORE-SHELL INTERFACIAL EXCHANGE INTERACTION J_{in}

Now, we turn to the study of the effect of the exchange interaction J_{in}/J_C linking core and shell spins. By using MFT and MCS we shown in Fig. 5, the

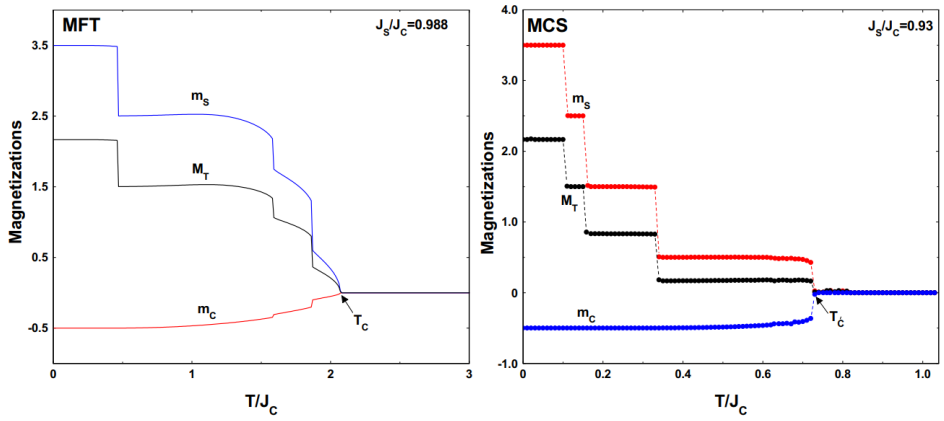

Fig. 4 – Sublattices magnetizations and the total magnetization and as a function of T/J_C for the case where $J_{in}/J_C = -0.2$, $D_S/J_C = -2$ and $J_S/J_C = 0.988$ by MFT and $J_S/J_C = 0.93$ by MCS.

phase diagrams in the (J_{in}/J_C, T/J_C) plane of the nanotube for $J_S/J_C = 0.2$ and $D_S/J_C = -2$. We notice that in both cases, there is no first order transition line, and that there is only a second-order transition line, which is an assembly of critical points that separates the ferrimagnetic phase from the paramagnetic one. The latter is accompanied by the appearance of the compensation temperature in the range $-1.07 \leq J_{in}/J_C < 0$ for MFT and in the range $-0.51 \leq J_{in}/J_C < 0$ for MCS. In addition, the T_C and T_{Comp} increase as the decreasing of J_{in}/J_C.

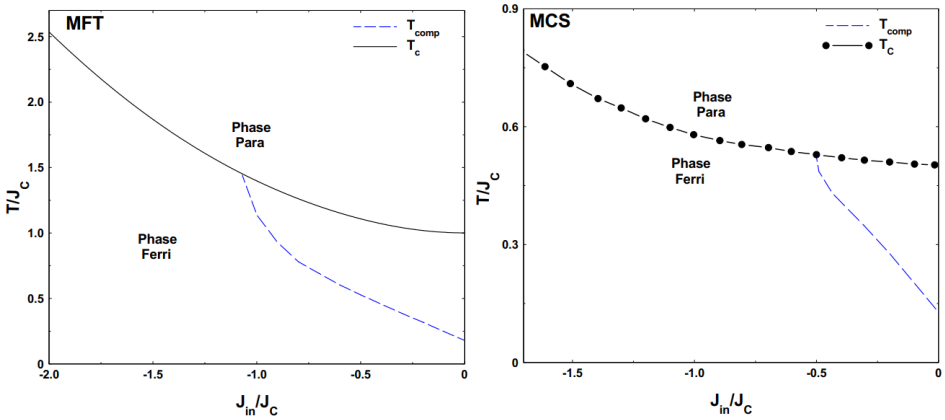

Fig. 5 – Phase diagrams of a nanotube system in the (J_{in}/J_C, T/J_C) plane when $J_S/J_C = 0.2$ and $D_S/J_C = -2$ by MFT and MCS.

To carefully affirm the appearance of the compensation phenomenon, we present typical results obtained by MFT and MCS of core, shell and total magnetizations

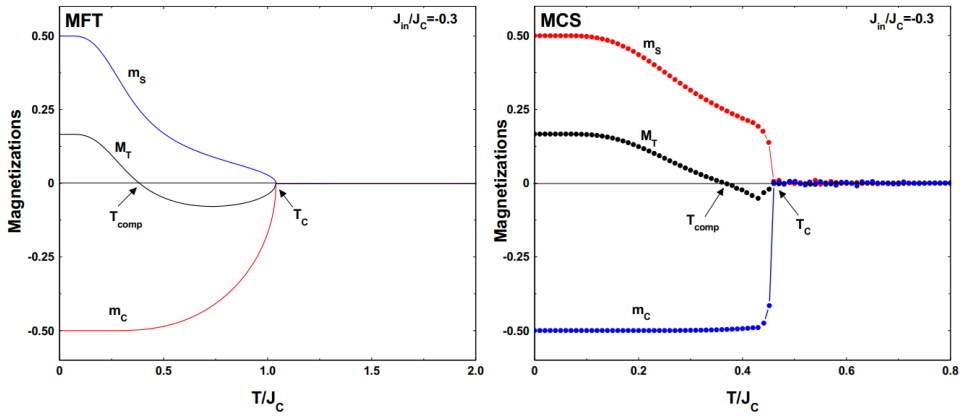

Fig. 6 – Sublattices magnetizations and the total magnetization and as a function of T/J_C for the case where $J_{in}/J_C = -0.3$, $D_S/J_C = -2$ and $J_S/J_C = 0.3$ by MFT and MCS

m_C, m_S and M_T as a function of temperature for $J_S/J_C = 0.2$, $D_S/J_C = -2$ and $J_{in}/J_C = -0.3$. As shown in the Fig. 6, it occur for both methods, m_C and m_S have opposite signs and each of these magnetizations starts from its saturation value and varies continuously until reaches the critical temperature. On the other hand, regarding the total magnetization M_T, we notice two important things, the first is that the saturation value of the latter is 0.16 given by $M_T = ((12 \times 0.5 - 6 \times 0.5)/18 = 0.16)$, and the second thing is that this magnetization cancels twice. The temperature for which it cancels first is associated with the compensation temperature while the other corresponds to the critical temperature.

Our results about the effect of exchange interaction J_{in}/J_C have been assured during the study of a cylindrical core-shell Ising nanowire by MCS of spin-1 and of spin-1/2 [39, 42] and also of the ferrimagnetic cylindrical Ising nanotube with spin-1/2 core and spin-3/2 shell [43].

3.3. EFFECT OF THE CRYSTAL FIELD D_S

Now, by keeping the J_S/J_C and J_{in}/J_C ratios constant ($J_S/J_C = 0.2$ and $J_{in}/J_C = -0.2$), we examine the influences of changing the crystal field as shown in Fig. 7. From this figure, we can observe that there exists a limit value ($(D_S/J_C)_C = -0.69$ for MFT and $(D_S/J_C)_C = -0.76$ for MCS) which indicates whether the system can display compensation behavior, such that for $D_S/J_C > (D_S/J_C)_C$ the system has no compensation temperature, whereas for $D_S/J_C \leq (D_S/J_C)_C$ it appears that it remains constant at the beginning and then increases rapidly until it meets the critical temperature line. We can also observe the appearance of the critical temperature T_C line, which divides the system into two parts. The first, located above this line, corresponds to the paramagnetic phase, and the other lo-

cated below, corresponds to the ferrimagnetic phase. What is more, at low temperature tree first order transitions lines are occur, and each of these lines ends with an critical end point E_i whose coordinates are, $E_1(D_S/J_C = -0.475, T/J_C = 0.22)$, $E_2(D_S/J_C = -0.437, T/J_C = 0.22)$ and $E_3(D_S/J_C = -0.425, T/J_C = 0.22)$ for MFT and $E_1(D_S/J_C = -0.48, T/J_C = 0.083)$, $E_2(D_S/J_C = -0.44, T/J_C = 0.083)$ and $E_3(D_S/J_C = -0.43, T/J_C = 0.058)$ for MCS.

To better understand what is represented in the phase diagram, we plot the magnetization curves versus temperature using the MFT and MCS. We provide an example where the magnetization displays the compensation temperature and another where the magnetizations undergo a first order phase transition. As we can see in Fig. 8, when the temperature increases, the surface magnetization decreases then the core magnetization increases until they meet and cancel out at the critical temperature. What is more, below this temperature, the total magnetization shows a point of compensation. Concerning the Fig. 9, it is clear that each magnetization is of surface or else the total magnetization makes three jumps first from the spin1/2 state to the spin 3/2 state, next from the spin 3/2 to the spin 5/2 and finally from the spin 5/2 state to the spin 7/2, in the sense that the crystal field increases, which show that the system exhibits three first order transitions lines.

It should be noted that the type of phase diagram obtained from the effect of the crystal field has been observed in other studies linked to Monte Carlo simulation of a hexagonal nanowire formed by a spin 1/2 core and spin 3/2 shell [44] and of a ferrimagnetic mixed-spin (3/2, 1/2) hexagonal Ising nanotube with core-shell structure by mean field theory [31]. We and the authors of these works found the compensation points and first-order phase transitions in the same region.

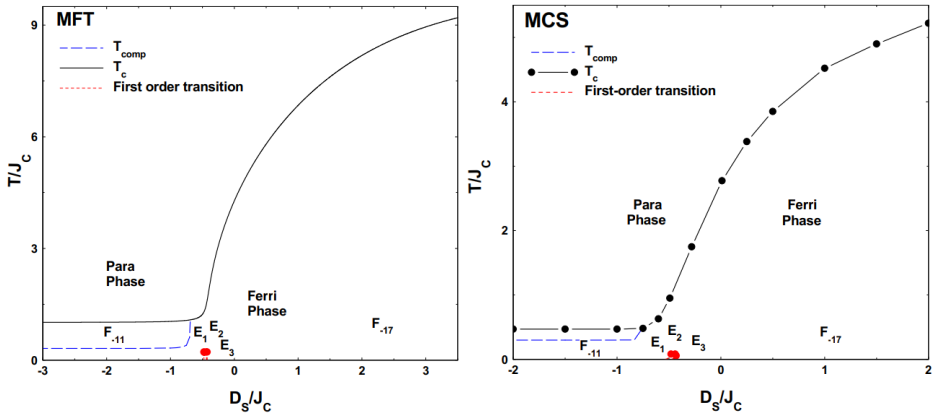

Fig. 7 – Phase diagrams of a nanotube system in the $(D_S/J_C, T/J_C)$ plane when $J_S/J_C = 0.2$ and $J_{in}/J_C = -0.2$ by MFT and MCS.

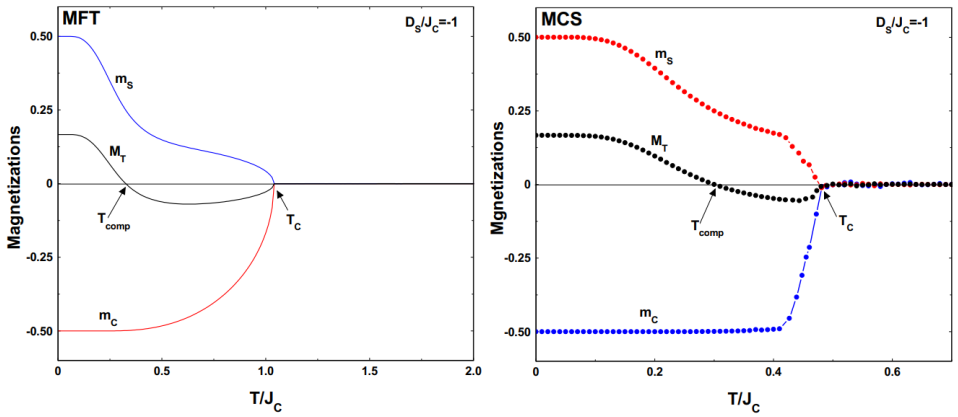

Fig. 8 – Sublattices magnetizations and the total magnetization and as a function of T/J_C for the case where $J_{in}/J_C = -0.2$, $D_S/J_C = -1$ and $J_S/J_C = 0.3$ by MFT and MCS.

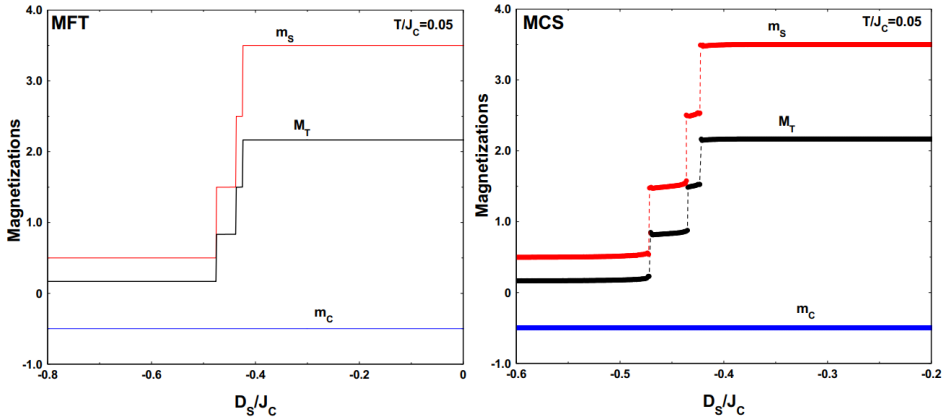

Fig. 9 – Sublattices magnetizations and the total magnetization and as a function of D_S/J_C for the case where $J_{in}/J_C = -0.2$, $T/J_C = 0.05$ and $J_S/J_C = 0.3$ by MFT and MCS.

4. CONCLUSION

In this work, the mean field theory and Monte Carlo simulation were employed to depict the effects of different parameters related to the Hamiltonian on the phase diagrams and magnetic properties of a hexagonal nanotube formed by a ferromagnetic core with spin-1/2 surrounded by a ferromagnetic shell with spin-7/2. We can conclude that the phase diagrams obtained by the two frameworks are topologically similar with some quantitative differences, such as the critical temperatures values acquired by MFT are bigger than those obtained by MCS. Furthermore, both methods show that the system can display first- and second-order phase transitions, critical end points and compensation behaviors. In parallel we have plotted magnetization

curves corresponding to the phase diagrams to confirm the results obtained in these diagrams.

REFERENCES

1. A. E. Berkowitz, R. H. Kodama, S. A. Makhlouf, F. T. Parker, F. E. Spada, E. J. McNiff Jr, S. Foner, J. Magn. Magn. Mater. **196**, 591 (1999).
2. S. Nie, S. R. Emory, Science **275**, 1102 (1997).
3. D. Kodamaa, K. Shinodab, K. Satoc, Y. Satoa, B. Jeyadevana, K. Tohji, J. Magn. Magn. Mater. **310**, 2396 (2007).
4. G. V. Kurlyandskaya, M. L. Sànchez, B. Hernando, V. M. Prida, P. Gorria, Appl. Phys. Lett. **82**, 3053 (2003).
5. H. Zeng, J. Li, J. P. Liu, Z. L. Wang, S. Sun, Nature **420**, 395 (2002).
6. C. Alexiou, A. Schmidt, R. Klein, P. Hulin, C. Bergemann , W. Arnold, J. Magn. Magn. Mater. **252**, 363 (2002).
7. A. Fert, L. Piraux, J. Magn. Magn. Mater. **200**, 338 (1999).
8. D. W. Elliott, W. X. Zhang, Environ. Sci. Technol. **35**, 4922 (2001).
9. S. Iijima, Nature **354**, 56 (1991).
10. H. Zhang, X. Zhang, J. Zhang, Z. Li, H. Sun, J. Magn. Magn. Mater. **342**, 69 (2013).
11. D. Zhou, L. Cai, F. Wen, F. Li, Chin. J. Chem. Phys. **20**, 821 (2007).
12. Y. L. Li, S. L. Tang, R. Xie, Y. Wang, M. Yang, J. L. Gao, W. B. Xia, Y. W. Du, Appl. Phys. Lett. **100**, 052402 (2012).
13. H. R. Liu, Q. F. Lu, X. F. Han, X. G. Liu, B. S. Xu, H. S. Ji, Appl. Surf. Sci. **258**, 7401 (2012).
14. C. F. Garnero, P. Gyawali, A. Lermechin, I. L. Pegg, J. Philip, J. Mater. Sci. Res **2**, 68 (2013).
15. F. S. Li, D. Zhou, T. Wang, Y. Wang, L. J. Song, C. T. Xu, J. Appl. Phys. **101**, 014309 (2007).
16. M. Steinhart, J. H. Wendorff, A. Greiner, R. B. Wehrspohn, K. Nielsch, J. Schilling, J. Choi, U. Gösele, Science **296**, 1997 (2002).
17. F. Taşkın, O. Canko, A. Erdinç, A. F. Yıldırım, Physica A **407**, 287 (2014).
18. Ü.Akınci, arXiv:1901.00328 [cond-mat.stat-mech] (2019).
19. Z. ElMaddahi, M. Y. El Hafidi, M. El Hafdi, Sci. Rep. **9**, 12364 (2019).
20. Z. ElMaddahi, M. El Hafidi, M. Y. El Hafidi, Physica E **122**, 114123 (2020).
21. T. Kaneyoshi, Phys. Status. Solidi. B **248**, 250 (2011).
22. R. G. B. Mendes, F. C. Sá Barreto, J. P. Santos, J. Magn. Magn. Mater. **471**, 365 (2019).
23. Y. Liu, W. Wang, D. Lv, X-R. Zhao, T. Huang, Z-Y. Wang, Physica B **541**, 79 (2018).
24. N. Maaouni, Z. Fadil, A. Mhirech, B. Kabouchi, L. Bahmad, W. Ousi Benomar, Solid State Commun. **321**, 114047 (2020).
25. R. Masrour, L. Bahmad, M. Hamedoun, A. Benyoussef, E. K. Hlil, Solid State Commun. **162**, 53 (2013).
26. J. P. Santos, Braz. J. Phys. **47**, 122 (2017).
27. E. M. Jalal, A. Lafhal, H. Saadi, A. Hasnaoui, M. Madani, M. El Bouziani, SPIN **13**, 2340005 (2023)
28. R. Masrour, A. Jabar, A. Benyoussef, M. Hamedoun, L. Bahmad, Physica B **472**, 19 (2015).
29. L. B. Drissi, S. Zriouel, J. Stat. Mech. **05**, 053206 (2016).
30. O. Dakir, A. El Kenz, A. Benyoussef, Physica A **426**, 45 (2015).
31. N. Hachem, I. A. Badrour, A. El Antari, A. Lafhal, M. Madani, M. El Bouziani, Chin. J. Phys. **71**,

12 (2021).
32. N. Hachem, Y. Al Qahoom, R. Aharrouch, M. Madani, M. El Bouziani, Rom. J. Phys. **67**, 612 (2022).
33. H. Falk, Am. J. Phys. **38**, 858 (1970).
34. N. Metropolis, A. W. Rosenbluth, M. N. Rosenbluth, A. H. Teller, E. Teller, J. Chem. Phys. **21**, 1087 (1953).
35. T. Kaneyoshi, Physica A **390**, 3697 (2011).
36. W. Wang, Y. Liu, Z. y. Gao, X. Zhao, Y. Yang, S. Yang, Physica E **101**, 110 (2018).
37. A. Zaim, M. Kerouad, Physica A **389**, 3435 (2010).
38. B. Boughazi, M. Boughrara, M. Kerouad, J. Magn. Magn. Mater. **354**, 173 (2014).
39. D. Lv, F. Wang, R. J. Liu, Q. Xue, S-X. Li, J. Alloys Compd. **701**, 935 (2017).
40. M. Boughrara , M. Kerouad, A. Zaim, J. Magn. Magn. Mater. **360**, 222 (2014).
41. A. Zaim, M. Kerouad, Y. ELAmraoui, J. Magn. Magn. Mater. **321**, 1077 (2009).
42. M. Boughrara, M. Kerouad, A. Zaim, J. Magn. Magn. Mater. **368**, 169 (2014).
43. N. Hachem, M. El Bouziani, SPIN **12**, 2250025 (2022).
44. B. Boughazi, M. Boughrara, M. Kerouad, Physica A **465**, 628 (2017).